A Study of Intraseasonal Temperature Variability in Southeastern South America

GUSTAVO NAUMANN

National Scientific and Technological Research Council (CONICET), and Department of Atmospheric and Oceanic Sciences, University of Buenos Aires, Buenos Aires, Argentina, and Climate Risk Management Unit, Joint Research Centre, European Commission, Ispra, Italy

WALTER M. VARGAS

National Scientific and Technological Research Council (CONICET), and Department of Atmospheric and Oceanic Sciences, University of Buenos Aires, Buenos Aires, Argentina

(Manuscript received 10 August 2011, in final form 14 February 2012)

ABSTRACT

The main goal of this work was to conduct an intraseasonal climate variability analysis using wavelet and principal component analysis over a southeastern South American daily maximum and minimum temperature series from the end of the nineteenth until the beginning of the twenty-first century. The analysis showed that there is a definite and coherent signal in the intraseasonal maximum and minimum temperatures. The most noticeable signal was observed during the winter months. The frequency of the intraseasonal signal was more complex for the maximum temperature, and in some stations, it displayed a bimodal distribution. A defined pattern that described a coherent variability between 30 and 60 days throughout the entire region was observed. This pattern potentially allows classification of the regional variability and adjustments to the temperature forecasting models on a daily basis.

1. Introduction

Processes or phenomena that evolve over time can generally be described by differential equations. If the solution of a dynamic system is not periodic, small uncertainties in the initial conditions can become so great as to make the forecast no better than a random prediction for the system. Current numerical weather forecasts have a predictability that is relatively accurate up to a period of approximately three weeks (Simmons and Hollingsworth 2002). Even if the predictability beyond three weeks is low, it is still of great interest, particularly when certain spatial or temporal structures are highly predictable over periods longer than three weeks.

Detecting these structures is difficult owing to the existence of unpredictable superimposed structures that dominate the effects (DelSole and Tippet 2007). For example, the evolution of a variable within a particular time window (a period of less than a season) can be highly predictable beyond three weeks, but this predictability can be difficult to detect in an analysis that takes the entire series into account (all seasons together). The same problem can occur for a particular region where the local predictability cannot be detected within a larger-scale analysis. Additionally, predictable components with periods longer than three weeks can be persistent and can therefore explain a large part of the variability in the monthly median values, even if the components only explain a small part of the daily variability (Shukla 1981a). Following this line of reasoning, Lorenz (1969), Shukla (1981b, 1984), Dirmeyer and Shukla (1993), and Goddard et al. (2001) have hypothesized that large-scale structures tend to be more persistent and, therefore, can be more predictable than smaller-scale processes. The characteristics of atmosphere–ocean systems that favor longer-term fluctuations are, by their very nature, limited to slower variations.

Therefore, there must be conditioning factors (both internal and external to the weather system) that, under certain conditions, can cause persistent physical processes that appear in the series as quasi cycles. This predictability, which exceeds three weeks, can be identified using the

Corresponding author address: Gustavo Naumann, Climate Risk Management Unit, Institute for Environment & Sustainability (IES), Joint Research Centre - European Commission, Via E. Fermi, 2749 - TP 280, I-21027 Ispra (VA), Italy.
E-mail: gustavo.naumann@jrc.ec.europa.eu

DOI: 10.1175/JCLI-D-11-00482.1

appropriate space and time filters. Several techniques have been used to identify predictable structures in atmospheric datasets. Barnett and Preisendorfer (1987) used a canonical correlation analysis to identify the relations between sea and air surface temperatures, and Lorenz (1965) used the singular value decomposition to identify the initial conditions that maximize the growth of the error. Deque (1988) and Renwick and Wallace (1995) used a principal component analysis to identify the most predictable patterns in operational forecast models. Venzke et al. (1999) used the relation between signal and noise in a multivariate analysis to identify predictable variables in a climate change scenario. Using a discriminant analysis, Schneider and Griffies (1999) identified the components that maximize the predictive power.

This work explores the structures that provide events with enhanced predictability at the intraseasonal time scale. An attempt is made to detect the intraseasonal signal by performing joint wavelet and principal component analyses. Long-term (from the end of the nineteenth century to the first decade of the twenty-first century) series of daily maximum and minimum temperatures obtained from reference stations in southeastern South America were used to obtain robust estimates. In particular, it is shown that the detection and discrimination of the intraseasonal variability modes can be used to construct monitoring tools and objective forecasting models. This method is particularly effective for time intervals in which the analyzed variable exhibits a substantial number of quasi periodicities (Mo 2001). The different modes that define the temporal evolution of temperature can also be used to improve the forecast by fitting time series models at each mode (Mann and Park 1999).

This work is organized as follows. The data and methods used are described in section 2. Section 3 discusses the wavelet spectral approximation over the temperature series. The interannual variation of the intraseasonal signal is described in section 4. Section 5 details the main oscillation trends within the intraseasonal scale. Finally, the main results are detailed in section 6.

2. Data and methods

a. Regional database

Series of daily maximum and minimum temperatures from 57 stations were provided by the Claris Project (Boulanger et al. 2010) and the National Weather Service of Argentina (Fig. 1 and Table 1). These series ensured a large quantity of reliable data for producing stable estimates and diagnostics of the transient oscillations over the reference series. A representative geographic distribution of stations was selected to include as many of the climatic regions of southern South America as possible and to cover a wide latitudinal range (23°–55°S). Eight of these stations (boldface in Table 1) have daily records ranging from the end of the nineteenth century to the first decade of the twenty-first century. These stations were used as the reference stations, and the main features of the present analysis are related to these stations. The National Centers for Environmental Prediction (NCEP)–Department of Energy (DOE) monthly mean reanalysis (Kanamitsu et al. 2002) was also used, including sea surface temperature (SST) and 850-hPa vector wind and air temperature anomalies.

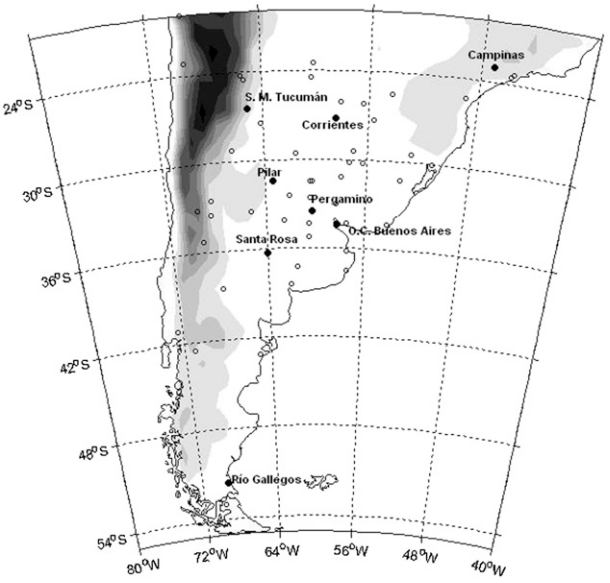

FIG. 1. Sampling stations used in this study (reference stations according to Table 1).

b. Wavelet analysis

Wavelet analysis is a tool that allows the analysis of spectral power variations within a time series. In general terms, this method allows the deconstruction of a time series in space–time frequency. In other words, the method determines the principal modes of variability and detects how these modes vary with time (Percival and Walden 2000). A complete description of wavelet analysis theory is found in Daubechies (1990, 1992), and complete descriptions of the application can be found in the studies by Foufoula-Georgiu and Kumar (1995) and Torrence and Compo (1998).

The wavelet transform can be used to analyze a series that has nonstationary spectral power for different frequencies. Assume that the time series X_n has the same time step for all t (i.e., constant Δt) and that there are $n = 0, \ldots, N - 1$ observations. A wavelet function $\psi_0(\eta)$ that depends on a dimensionless time parameter η is used to begin the analysis. For a function to be suitable as

TABLE 1. The descriptions, geographical locations, and observation periods for the sampling stations in the regional database. The reference stations are highlighted in bold type.

Country	Region	Lat	Lon	Start	End
Chile	Arica	−18.12	−69.52	1967	2005
Brazil	**Campinas**	**−23**	**−47.12**	**1890**	**2003**
Chile	Antofagasta	−23.15	−69.55	1967	2005
Brazil	Sao Paulo	−23.37	−45.61	1951	1997
Paraguay	M. Estigarribia	−23.49	−60.22	1950	1999
Brazil	Santos	−23.56	−45.82	1951	2000
Argentina	Jujuy	−24.23	−65.5	1967	2006
Argentina	Las Lomitas	−24.42	−60.35	1956	2006
Argentina	Salta	−24.51	−65.29	1956	2006
Brazil	Curitiba	−25.31	−48.89	1951	1997
Argentina	Iguazu aero	−25.44	−54.28	1961	2004
Argentina	Formosa	−26.12	−58.14	1962	2006
Paraguay	Villarica	−26.15	−56.43	1956	1999
Argentina	**Tucumán**	**−26.8**	**−65.2**	**1891**	**2007**
Argentina	Posadas	−27.22	−55.58	1956	2006
Argentina	**Corrientes**	**−27.43**	**−58.74**	**1894**	**2007**
Argentina	Sgo. Del Estero	−27.46	−64.18	1956	2006
Argentina	La Rioja	−29.23	−66.49	1956	2006
Argentina	P de los libres	−29.41	−57.09	1956	2006
Brazil	Santa Maria	−29.43	−52.58	1961	1996
Argentina	Ceres	−29.53	−61.57	1956	2006
Brazil	Porto Alegre	−30	−50.89	1951	1996
Argentina	Monte Caseros	−30.16	−57.39	1959	2006
Uruguay	Artigas	−30.23	−56.3	1960	2002
Argentina	Concordia	−31.18	−58.01	1962	2006
Brazil	Bague	−31.23	−53.3	1961	1997
Argentina	Sauce Viejo	−31.42	−60.49	1958	2006
Argentina	Paraná	−31.47	−60.29	1956	2006
Argentina	**Pilar**	**−31.64**	**−63.85**	**1931**	**2007**
Argentina	Marcos Juarez	−32.42	−62.09	1956	2006
Argentina	Mendoza	−32.5	−68.47	1959	2006
Argentina	Rosario	−32.55	−60.47	1950	2006
Argentina	Gualeguaychu	−33	−58.37	1956	2006
Chile	Qta Normal	−33.15	−69.64	1968	2005
Argentina	Villa Reynolds	−33.44	−65.23	1956	2006
Argentina	San Martin	−33.5	−68.52	1956	2006
Argentina	**Pergamino**	**−33.9**	**−60.53**	**1931**	**2007**
Argentina	Laboulaye	−34.08	−62.62	1950	2006
Uruguay	La Estanzuela	−34.27	−57.5	1960	2002
Uruguay	Rocha	−34.29	−54.18	1960	2002
Argentina	Junin	−34.33	−60.55	1958	2006
Argentina	Palomar	−34.36	−58.36	1956	2006
Argentina	Ezeiza	−34.49	−58.32	1956	2006
Argentina	**Buenos Aires**	**−34.57**	**−58.42**	**1906**	**2007**
Argentina	Nueve de julio	−35.27	−60.53	1950	2006
Argentina	Malargue	−35.3	−69.35	1956	2006
Argentina	Dolores	−36.21	−57.44	1956	2006
Argentina	**Santa Rosa**	**−36.54**	**−64.26**	**1937**	**2007**
Argentina	Cnel. Suarez	−37.26	−61.53	1956	2006
Argentina	Mar del Plata	−37.56	−57.35	1956	2006
Argentina	Bahia Blanca	−38.44	−62.1	1956	2006
Argentina	Neuquen	−38.57	−68.08	1959	2006
Chile	Pto Montt	−41.15	−72.43	1967	2005
Argentina	Esquel	−42.56	−71.09	1961	2006
Argentina	Trelew	−43.12	−65.16	1956	2006
Argentina	**Río Gallegos**	**−51.99**	**−69.45**	**1896**	**2007**
Chile	Pta. Arenas	−53	−69.7	1967	2005

a wavelet, it must have a mean equal to zero and be located within the time and frequency ranges (Farge 1992). The Morlet wavelet function consists of a planar wave modulated by a Gaussian function:

$$\psi_0(\eta) = \pi^{-1/4} e^{i\omega_0 \eta} e^{-\eta^2/2}, \tag{1}$$

where ω_0 is a dimensionless frequency.

The continuous wavelet transform of a discrete data sequence (X_n) is defined as the convolution of X_n with respect to $\psi_0(\eta)$:

$$W_n(s) = \sum_{n'=0}^{N-1} X_n' \psi^* \left[\frac{(n' - n)\Delta t}{s} \right], \tag{2}$$

where the asterisk indicates the complex conjugate. Starting with variations in the wavelet scale s and translating the index η in time, it is possible to build a two-dimensional diagram that shows the spectral power for different frequencies and the variation of this power with respect to time. More details regarding the approximation of the continuous wavelet transform can be found in Kaiser (1994).

Within the continuity limits and by the convolution theorem, the wavelet transform is the inverse of the Fourier transform of the product:

$$W_n(s) = \sum_{k=0}^{N-1} \hat{X}_n \hat{\psi}^*(s\omega_k) e^{i\omega_k n \Delta t}, \tag{3}$$

where

$$\hat{X}_k = \frac{1}{N} \sum_{n=0}^{N-1} X_n e^{-2\pi i k n / N} \tag{4}$$

and $k = 0, \ldots, N - 1$ is the frequency index.

A wavelet analysis can be used to examine spectral power fluctuations over a range of scales (bands). For this purpose, the average spectral power can be defined as a function of the scale as the weighted sum of the wavelet spectral power between scales s_1 and s_2:

$$\overline{W}_n^2 = \frac{\Delta j \Delta t}{c\Delta} \sum_{j=j1}^{j2} \frac{|W_n(s_j)|^2}{s_j}. \tag{5}$$

A time series is obtained as a result of (5) that represents the median variance for the bandwidth in question. Therefore, the spectral power averaged by scale can be used to examine the modulation of one series by another or one frequency by another within the same time series.

Using this method, it is possible to identify the periods in which more persistent phenomena appear. These periods

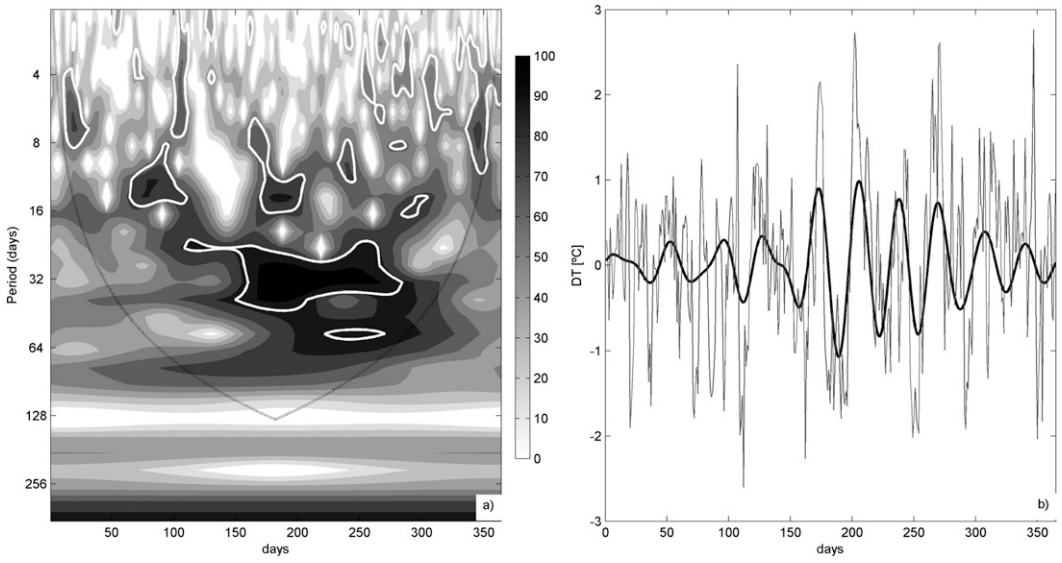

FIG. 2. (a) The estimated wavelet spectrum ($°C^2$) for the minimum temperature in S. M. de Tucumán in 1976. The white contours represent the 5% significance level with respect to an autoregressive model. (b) The minimum temperature anomalies (thin line) and a reconstruction of the anomalies in the bandwidth between 30 and 60 days (bold line).

are identified in the time series by the presence of quasi cycles. Therefore, if there is a recurring periodicity, it is possible to investigate the time intervals over which this periodicity had a greater influence by monitoring the spectral densities associated with the individual periods.

3. Estimation of the intraseasonal variation over the reference series

Several works have studied intraseasonal variation in southern South America, especially the variation in precipitation (Liebmann et al. 2004; Gonzalez et al. 2008). Additionally, Minetti and Vargas (1997), Cerne and Vera (2010), and Naumann and Vargas (2010) have demonstrated the existence of a modulation in the intraseasonal fluctuations of temperature anomalies in the Argentinean tropics and extratropics due to the different phases of the El Niño–Southern Oscillation (ENSO), the South Atlantic convergence zone (SACZ), and the Madden–Julian oscillation (MJO). A wavelet spectral analysis of the daily maximum and minimum temperature series was performed to detect the thermal structures that produced persistent phenomena. From this analysis, the main spectral characteristics of the preferential bandwidths were determined within the intraseasonal scale.

Figure 2 shows an example of a wavelet spectrum for the 1976 Tucumán minimum temperature series that uses the Morlet basis. This spectrum exhibits peaks related to the synoptic variability and significant spectral densities for the quasi cycles of periods between 25 and 50 days, indicating that cold/hot surges are favored during winter. This concept is related to the appearance of physical processes or circulation patterns that tend to modulate the meridional heat transport with a particular frequency within the intraseasonal spectrum (Ghil and Mo 1991a,b; Higgins and Mo 1997).

Given that the wavelet transform is also a band filter with a known response function (i.e., the wavelet function), it is possible to reconstruct the original time series or, simply, the characteristic of the series for the desired bandwidth. In this case, the reconstructed time series is the sum of the real part of the wavelet transform over the desired scales:

$$x'_n = \frac{\delta_j \delta_t^{1/2}}{c_\delta \psi_0(0)} \sum_{j=j1}^{j2} \frac{\Re\{W_n(s_j)\}}{s_j^{1/2}}. \tag{6}$$

This filter has a response function given by the sum of the wavelet functions between scales j_1 and j_2.

Figure 2b shows the anomalies of the 1976 minimum temperatures and the reconstruction of the series in the bandwidth with periods between 30 and 60 days according to Eq. (6). This reconstruction can be interpreted as the contribution to the amplitude of the daily anomalies from the variability with periods between 30 and 60 days. The figure shows that during the winter (the season that displays the greatest spectral density), the amplitude of the reconstructed anomalies in the intraseasonal range begins to increase stepwise and in phase with the total anomalies. In this case, the reconstructed

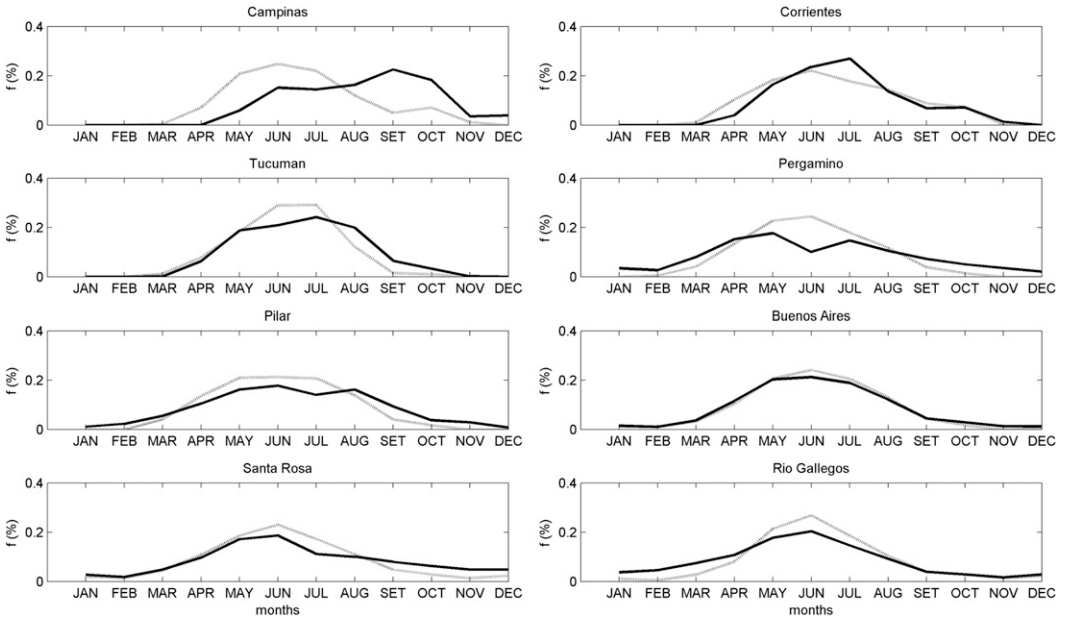

FIG. 3. The annual distribution of the frequency of significant maximum (black bold line) and minimum temperature (gray line) spectral densities in the bandwidth between 30 and 60 days.

amplitude increases significantly between the months of May and September, displaying an amplitude near 1°C. This observation indicates that, in some cases, intraseasonal variability represents more than 40% of the total variability. Following this line of reasoning, Naumann et al. (2011) showed the existence of fluctuations with periods between 20 and 90 days over the series of daily temperatures, with a greater frequency observed in fluctuations with periods between 30 and 60 days. Similar results for the region have been found by Ghil and Mo (1991b), Minetti (1991), and Minetti and Vargas (2005).

Therefore, the diagnosis and identification of the processes in which the intraseasonal variations tend to become evident will play an important role when used as inputs to stochastic or dynamic forecasting models (Straus and Shukla 1981; Lau and Chang 1992; Doblas-Reyes et al. 1998).

Figure 2 shows that the variability in the 30- and 60-day bands for 1976 displays greater spectral energy during winter months. This result raises the question of whether this type of linear or nonlinear effect tends to be observed in a particular season. Figure 3 shows the distribution of the occurrence of significant spectral densities in the bandwidth between 30 and 60 days as a function of the month of the year. Significance was assessed using a red noise (autoregressive lag 1) background spectrum. For most of the reference stations, including the maximum and minimum temperatures, it is clear that the winter months display the greatest frequency for this variability. For the maximum temperature, the frequency of this intraseasonal signal appears to be slightly more complex; in some sampling stations (Campinas, Tucumán, Pergamino, Pilar, and Santa Rosa), this characteristic tends to have a bimodal distribution. Here, the maxima tend to occur at the beginning and end of winter. In locations where this pattern is observed, the maxima are especially associated with the beginning and end of a dry season (Vargas et al. 2011).

From a regional perspective, Fig. 4 shows the spatial distribution of the day of the year with the greatest number of significant spectral densities in the 30- to 60-day bandwidth using the regional database. Again, the frequency of significant densities was calculated using a red noise background spectrum for each day. Indeed, the largest signal in this bandwidth is seen over the maximum temperature between the end of autumn and the start of winter in central Argentina and southern Brazil, while the greatest amplitude for Patagonia is recorded in the spring (October–November). The behavior of this signal is more homogeneous for the minimum temperature, with the greatest frequency of days with a signal occurring within a 15-day range centered on 1 July (the approximate day when the annual temperature minimum is recorded). The spatial heterogeneity observed in the maximum temperature may be directly associated with the influence that cloud cover has on the maximum temperature (Karl et al. 1993), while the minimum temperature appears to be independent of this effect.

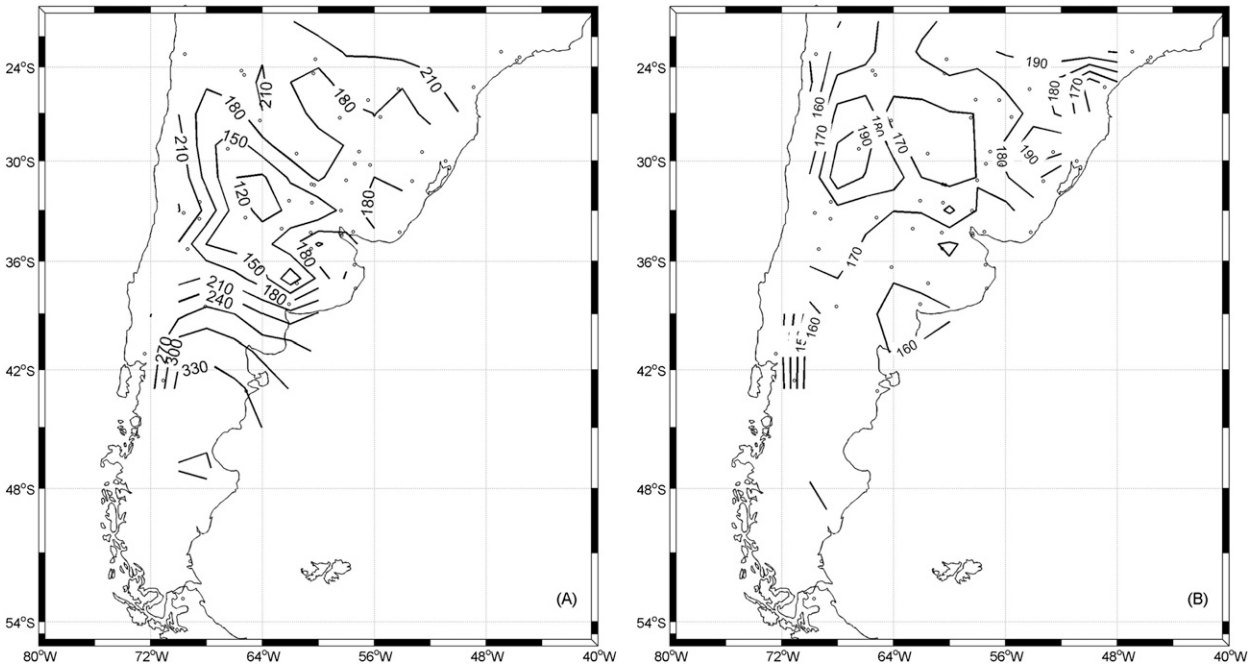

FIG. 4. The spatial distribution of the day of the year with the greatest number of significant reference station (a) maximum temperature and (b) minimum temperature spectral densities in the bandwidth between 30 and 60 days.

4. Interannual variation of the intraseasonal spectral estimation

The main mode of intraseasonal oscillation (30–90 days) is seen in the periods between 30 and 60 days (Ghil and Mo 1991b; Madden and Julian 1994). This mode, which is seen over different weather system variables, is forced by different persistent circulation patterns that respond to changes in the boundary conditions of the system. In addition, in the region Naumann and Vargas (2010) found that the temperatures in tropical/subtropical southeastern South America are modulated by the Madden–Julian oscillation. However, this type of oscillation has a transient effect on seasonal and interannual variations. In other words, a phenomenon of this kind does not have the same impact on each variable (in magnitude or in duration) every year.

This phenomenon is not observed in all years and has a probability of occurrence between 30% and 50%, depending on the location. Given this variability, some periods in which this intraseasonal perturbation occurs more frequently and displays greater amplitude are observed (results not shown). During the 1950s and 1970s and at the end of the 1980s, the maximum amplitude of this oscillation was greater than 3°C.

In contrast, a regional coherence is observed in the circulation patterns that are associated with this kind of variability. To support this statement, the monthly mean composite of wind and temperature anomalies (Figs. 5a–c) was calculated for seasons that exhibited intraseasonal variability at six or more of the eight reference stations for both maximum and minimum temperatures. For these seasons, a predominance of southern winds during May is observed, mainly conducted by a blocking high pressure system located near the western coasts of southern South America and adjacent to a low pressure system positioned in the South Atlantic. This pattern leads to below-normal temperatures across the southern part of the continent (Fig. 5a). For June (Fig. 5b) the warm advection observed over the eastern part of the continent is mainly due to the intensification of the South Atlantic semipermanent anticyclone. This effect is not observed over Patagonia, a region that shows negative temperature anomalies. During July the whole continent is again covered with negative temperature anomalies conducted by a cyclonic system located in the southern Atlantic Ocean (Fig. 5c). This observation leads to the inference that the processes that modulate this variability are largely attributable to surges of polar air traveling toward the tropics or, conversely, to the persistence of tropical air (heat waves). It is also noted that the SST anomalies (Fig. 5d) related to these events are associated with cold anomalies in the western equatorial Pacific (La Niña events) and with warm SST anomalies near the coasts of southern Brazil and Uruguay. This statement agrees with the findings by Sinclair et al. (1997), who documented links between

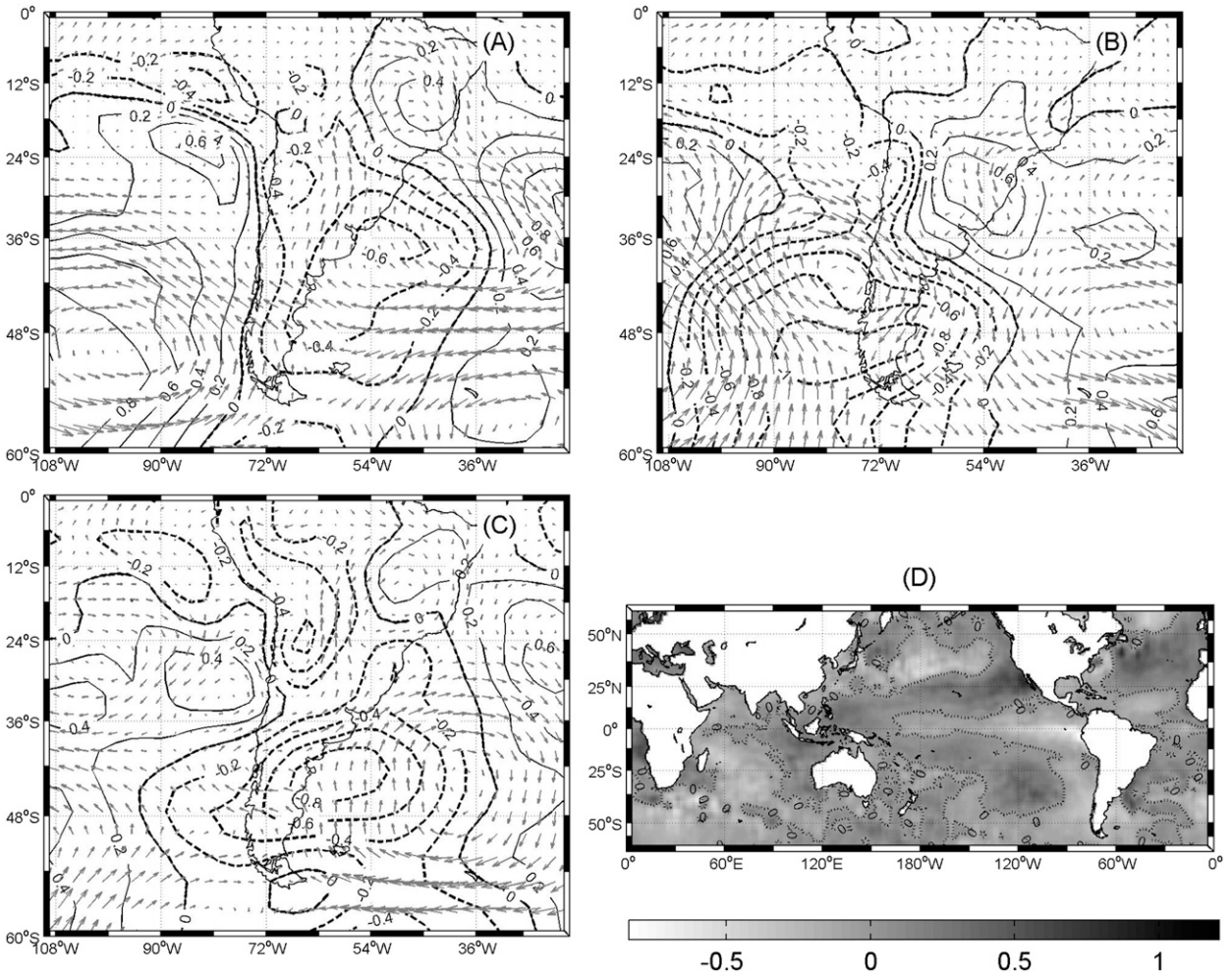

FIG. 5. The composite vector of wind (m s^{-1}) and temperature anomalies (°C) at 850 hPa for the seasons with intraseasonal temperature signals in at least six of the eight reference stations during (a) May, (b) June, and (c) July, and (d) the May–July sea surface temperature-mean composite.

ENSO and weather system tracks characterized by a coherent cyclone response to ENSO, especially during austral winter. During El Niño winters a 20% increase in cyclones occur in a broad band extending southeastward from the subtropical Pacific toward South America, while during La Niña these patterns are almost exactly reversed. Grimm et al. (2000) state the circulation anomalies during ENSO events are the near equivalent of barotropic dipolelike circulation anomalies over the Pacific and Atlantic Oceans, with reversed polarity. However, the centers of the anomalies undergo some changes of magnitude and shifts in position.

Regarding the interdecadal variability of these circulation patterns, Silvestri and Vera (2009) found changes in the typical hemispheric circulation pattern associated with the southern annular mode (SAM), particularly over South America and Australia, between the 1960s–1970s and the 1980s–1990s. During the first decades, the SAM positive phase is associated with an anomalous anticyclonic circulation that developed in the southwestern subtropical Atlantic. During the latter decades, however, the anticyclonic anomaly induced by the SAM positive phase covers most of southern South America and the adjacent Atlantic, producing weakened moisture convergence and a positive temperature anomaly advection over southern South America.

An interdecadal variability is also observed in the intraseasonal variability studied. Figure 6 shows the fields associated with the maximum amplitudes [reconstructed according to Eq. (6)] of the waves with periods between 30 and 60 days. The figure shows a distribution characterized by a meridional gradient with few spatial variations and by temperature anomaly amplitudes between 2 and 3°C over nearly the entire region. The regions that

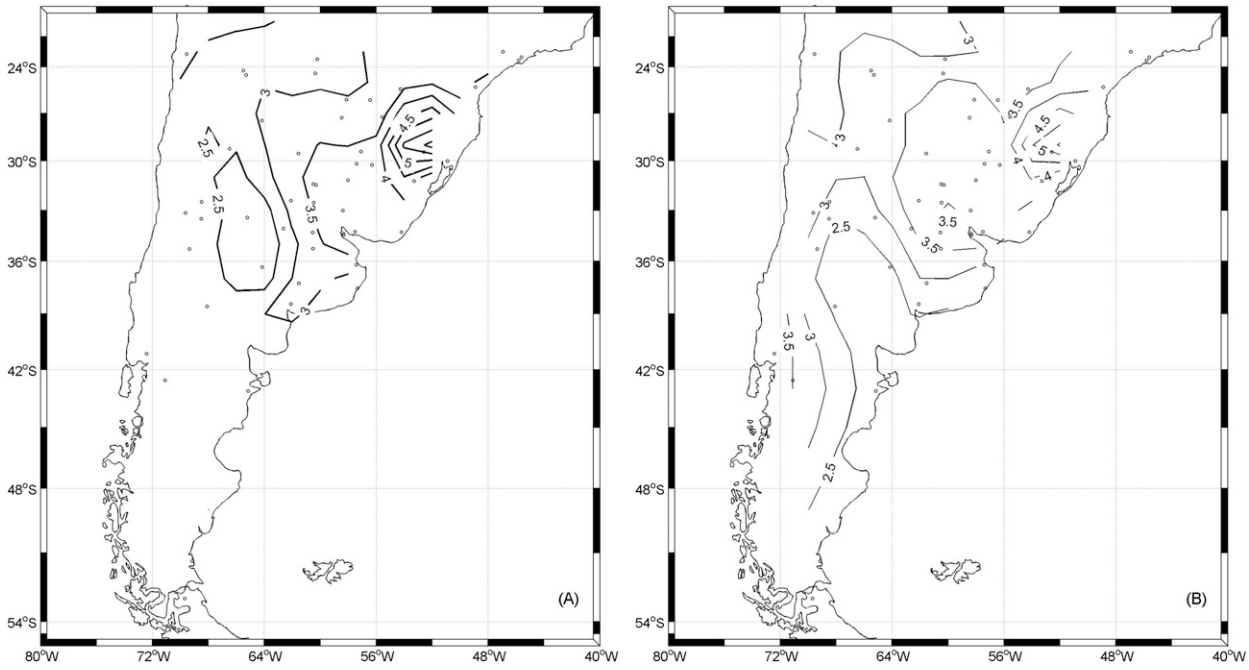

FIG. 6. The spatial distribution of the maximum amplitude (°C) of the oscillations between 30 and 60 days for the (a) maximum and (b) minimum temperatures.

show the greatest differences are northeast Argentina and southern Brazil, where maximum amplitudes near 5°C are observed.

Considering the years during which these maxima occur, Fig. 7 shows the isochrones relative to the occurrence of the maximum oscillation amplitude (i.e., the maximum intraseasonal signal) between 30 and 60 days over the maximum and minimum temperatures. It can be seen that the greatest intraseasonal signals in northern and central Argentina occurred during the 1970s, while the maxima for northeastern Argentina and southern Brazil were recorded during the 1990s. These results support the hypothesis of a consistent signal in the occurrence pattern of the intraseasonal mode. In addition, the difference between the behavior patterns in northwestern Argentina and southern Brazil is highlighted, with the latter being the region where the ENSO and MJO had greater impacts on precipitation and temperature (Barros and Silvestri 2002; Penalba and Vargas 2004; Naumann and Vargas 2010).

5. Main modes of oscillation at the intraseasonal scale

Recognizing patterns or, in this case, oscillation modes depends on the selection and extraction of characteristics from the analyzed information. The main goal of the classification technique is to obtain a reduction in the spatial dimensions associated with the original data. The following sections detail the results of classifying the intraseasonal oscillation modes of the daily temperatures using principal component analysis. This method was applied over the series of temperature anomalies reconstructed using Eq. (7) in the 30- to 60-day bandwidth for the years that recorded a significant spectral density for that region of the spectrum.

The principal component analysis was performed by computing the eigenvectors and eigenvalues of a correlation matrix computed from the original groups in the intraseasonal signal reconstructed from the maximum and minimum daily temperature series. It was then possible to extract the coherent variations from the original groups and create new groups using the original time series data and the eigenvectors. Figure 8 shows the variance explained by each principal component (PC) over the reconstruction of the maximum and minimum temperature anomalies in the bandwidth between 30 and 60 days. A homogeneous regional behavior can be seen for both variables. Generally, the first component explains 14%–18% of the total variance, with the minimum temperature having the most identifiable intraseasonal oscillation patterns. In addition, the first three PCs explain more than 40% of the variance in the region. Accounting for the transient characteristics of these waves, this degree of explained variance suggests the existence of a stable pattern. This stable pattern will

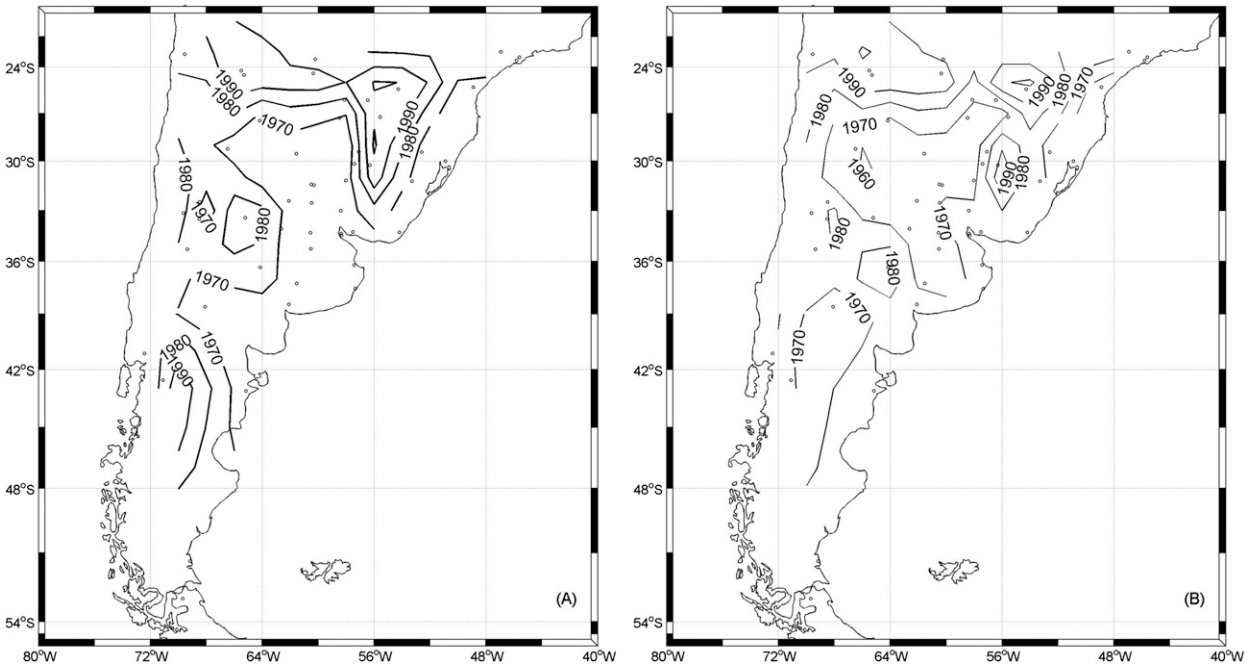

FIG. 7. The isochrones (years) of the maximum amplitude of the oscillations between 30 and 60 days for the (a) maximum and (b) minimum temperatures.

in turn allow identification of a conceptual model for the general characteristics of this type of oscillation.

Figure 9a shows the first PC for the reference stations. A strong regional coherence can again be seen, and the pattern appears to be the same for all reference stations. This mode is characterized by an increase in the intraseasonal signal for both maximum and minimum temperatures during winter. Generally, the beginning of this

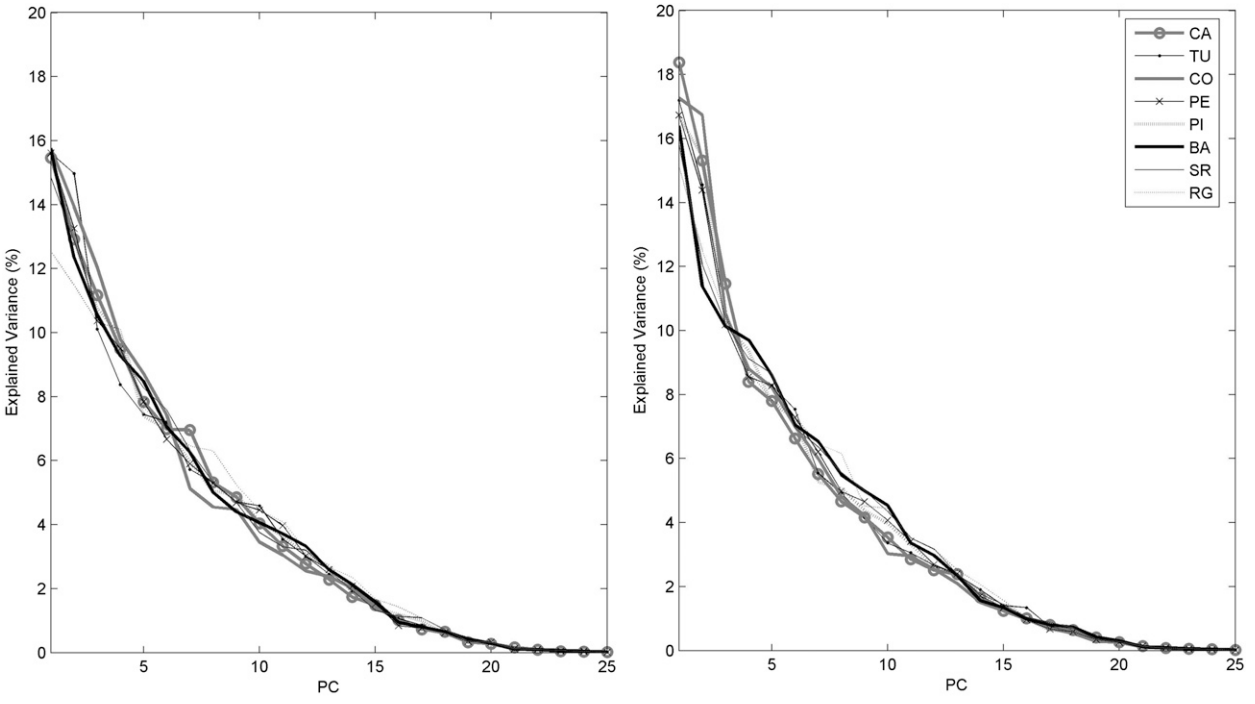

FIG. 8. The variance explained by each principal component (PC) of the filtered (a) maximum and (b) minimum temperature anomalies for the bandwidth between 30 and 60 days.

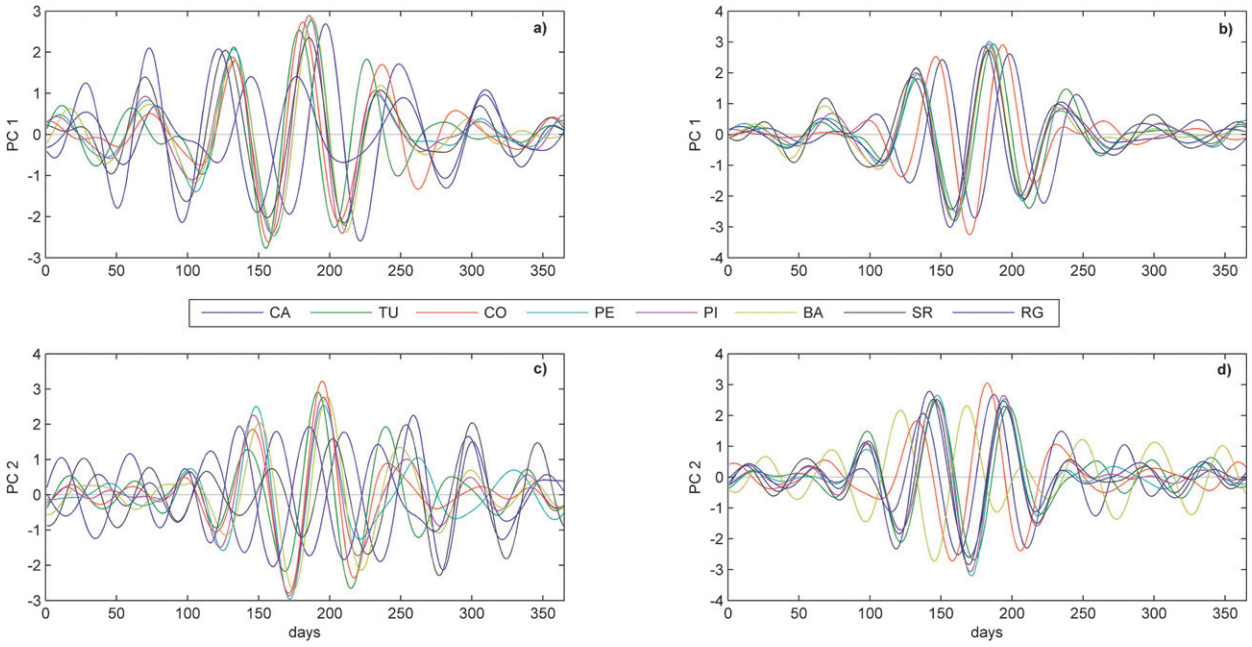

FIG. 9. PC1 of the (a) maximum and (b) minimum temperatures and PC2 of the (c) maximum and (d) minimum temperatures, for the reference stations listed in bold font in Table 1.

signal for the two variables is associated with an intense warm (cold) surge of air followed 30 days later by a cold (warm) surge of great intensity. A warm (cold) surge is observed in July, and another intense cold (warm) surge is recorded approximately 30 days later. Before and after this period, the intraseasonal signal tends to be incoherent and to have negligible amplitude.

The model previously described is the main mode observed, and it results from modulation in the intraseasonal temperature band. This result allows identification of the seasons of the year in which the regional maximum warm and cold surges are expected and the extent of the surges' magnitudes. This description is valid for most tropical stations and Campinas and Corrientes, with a 15-day lag; the first warm surge is observed in the first days of June.

By analyzing the second PC (Fig. 9b), it can be seen that the regional coherence for the maximum temperature is not as strong as that seen with the first PC. However, a cold (warm) surge is seen in the middle of June followed 30 days later by a warm (cold) surge. Finally, another cold (warm) surge is observed during the middle of August. However, the minimum temperature displays a more homogeneous signal for the second PC. Here, the regional model can be described as having intense cold surges during the months of April, June, and August and warm surges in May and July.

The information contained in the first two principal components describes the effect of large-scale circulation patterns on the thermal properties of surface air in the region. These generally large-scale processes tend, under certain conditions, to favor the meridional heat transport in the form of intraseasonal quasiperiodicities that could persist for a period of one to three seasons.

6. Conclusions

This study is an empirical analysis using historical daily data, not a test of a specific dynamical hypothesis. For this reason, the conclusions drawn must be tentative. Nevertheless, we can make several observations on the basis of this analysis.

The identification of spectral structures in time that result from transient physical phenomena allows the detection of periods in which the predictability of the system increases, thus improving objective forecasts.

For the maximum and minimum temperatures, the winter months displayed the greatest intraseasonal variability signal. The intraseasonal signal pattern was slightly more complex for the maximum temperature. For some stations (Campinas, Tucumán, Pergamino, Pilar, and Santa Rosa), the pattern tended to have a bimodal distribution with maxima at the beginning and end of winter.

The coherent spatiotemporal patterns of intraseasonal temperature variation revealed by this analysis may have more than one possible explanation. Nevertheless, the coincidence of significant ENSO, MJO, and SAM variability with these oscillation modes in temperature suggests

possible dynamic linkages that could be investigated in coupled ocean–atmosphere model experiments.

In the classification based on the principal component analysis, there was a main mode characterized by an increase in the intraseasonal signal during winter for both maximum and minimum temperatures. Generally, the beginning of this signal was associated with an intense warm (cold) surge of air followed 30 days later by an intense cold (warm) surge. Then, a warm (cold) surge was observed in July. Finally, approximately 30 days later, another intense cold (warm) outbreak was recorded. The intraseasonal signal tended to be incoherent and to have negligible amplitude before and after this period.

The combination of wavelet analysis with PCA makes it possible to apply the spectral methods discussed herein to seasonal temperature prediction. The key idea is that each significant oscillation mode obtained from analysis is a narrowband time series; the mode can therefore be predicted fairly robustly by computing a low-order autoregressive process that fits this mode over the time interval available (Naumann et al. 2011). The separate reconstructed mode predictions can then be combined to form a partial reconstruction of the future evolution of the entire time series (Keppenne and Ghil 1993; Vautard et al. 1992). The accuracy of the prediction depends, in either case, on the extent to which the available data from the past determine the regular, that is, periodic and multiple periodic, behavior of the time series (Mann and Park 1999).

Acknowledgments. This research was sponsored by Projects UBA X-228, CONICET PIP 112-200801-00762, and FONCyT PICT 2008-1820.

REFERENCES

Barnett, T. P., and R. Preisendorfer, 1987: Origins and levels of monthly and seasonal forecast skill for United States surface air temperatures determined by canonical correlation analysis. *Mon. Wea. Rev.,* **115,** 1825–1850.

Barros, V. R., and G. E. Silvestri, 2002: The relationship between sea surface temperature at the subtropical south-central Pacific and precipitation in southeastern South America. *J. Climate,* **15,** 251–267.

Boulanger, J., and Coauthors, 2010: A Europe-South America network for climate change assessment and impact studies. *Climatic Change,* **98,** 307–329.

Cerne, S. B., and C. S. Vera, 2010: Influence of the intraseasonal variability on heat waves in subtropical South America. *Climate Dyn.,* **36,** 1–13.

Daubechies, I., 1990: The wavelet transform time-frequency localization and signal analysis. *IEEE Trans. Inf. Theory,* **36,** 961–1004.

——, 1992: *Ten Lectures on Wavelets*. Society for Industrial and Applied Mathematics, 357 pp.

DelSole, T., and M. K. Tippett, 2007: Predictability: Recent insights from information theory. *Rev. Geophys.,* **45,** RG4002, doi:10.1029/2006RG000202.

Deque, M., 1988: 10-day predictability of the northern hemisphere winter 500-mb height by the ECMWF operational model. *Tellus,* **40A,** 26–36.

Dirmeyer, P. A., and J. Shukla, 1993: Observational and modelling studies of the influence of soil moisture anomalies on atmospheric circulation. *Prediction of Interannual Climate Variations,* J. Shukla, Ed., NATO ASI Series, Springer, 1–23.

Doblas-Reyes, F. J., M. Déqué, F. Valero, and D. B. Stephenson, 1998: North Atlantic wintertime intraseasonal variability and its sensitivity to GCM horizontal resolution. *Tellus,* **50A,** 573–595.

Farge, M., 1992: Wavelet transforms and their applications to turbulence. *Annu. Rev. Fluid Mech.,* **24,** 395–457.

Foufoula-Georgiou, E., and P. Kumar, Eds., 1995: *Wavelets in Geophysics*. Academic Press, 373 pp.

Ghil, M., and K. Mo, 1991a: Intraseasonal oscillations in the global atmosphere. Part I: Northern Hemisphere and tropics. *J. Atmos. Sci.,* **48,** 752–779.

——, and ——, 1991b: Intraseasonal oscillations in the global atmosphere. Part II: Southern Hemisphere. *J. Atmos. Sci.,* **48,** 780–790.

Goddard, L., S. J. Mason, S. E. Zebiak, C. F. Ropelewski, R. Basher, and M. A. Cane, 2001: Current approaches to seasonal-to-interannual climate predictions. *Int. J. Climatol.,* **21,** 1111–1152.

Gonzalez, P., C. Vera, B. Liebmann, and G. Kiladis, 2008: Intraseasonal variability in subtropical South America as depicted by precipitation data. *Climate Dyn.,* **30,** 727–744.

Grimm, A. M., V. R. Barros, and M. E. Doyle, 2000: Climate variability in southern South America associated with El Niño and La Niña events. *J. Climate,* **13,** 35–58.

Higgins, R. W., and K. C. Mo, 1997: Persistent North Pacific circulation anomalies and the tropical intraseasonal oscillation. *J. Climate,* **10,** 223–244.

Kaiser, G., 1994: *A Friendly Guide to Wavelets*. Birkhäuser, 300 pp.

Kanamitsu, M., W. Ebisuzaki, J. Woollen, S.-K. Yang, J. J. Hnilo, M. Fiorino, and G. L. Potter, 2002: NCEP–DOE AMIP-II Reanalysis (R-2). *Bull. Amer. Meteor. Soc.,* **83,** 1631–1643.

Karl, T. R., and Coauthors, 1993: A new perspective on recent global warming—Asymmetric trends of daily maximum and minimum temperature. *Bull. Amer. Meteor. Soc.,* **74,** 1007–1023.

Keppenne, C. L., and M. Ghil, 1993: Adaptive filtering and prediction of noisy multivariate signals: An application to subannual variability in atmospheric angular momentum. *Int. J. Bifurcat. Chaos,* **3,** 625–634.

Lau, K.-M., and F. C. Chang, 1992: Tropical intraseasonal characteristics of large-scale and extended range forecasts in the NMC operation model. *J. Climate,* **5,** 1365–1378.

Liebmann, B., G. N. Kiladis, C. Vera, A. C. Saulo, and L. M. V. Carvalho, 2004: Subseasonal variations of rainfall in South America in the vicinity of the low-level jet east of the Andes and comparison to those in the South Atlantic convergence zone. *J. Climate,* **17,** 3829–3842.

Lorenz, E. N., 1965: A study of the predictability of a 28-variable atmospheric model. *Tellus,* **17,** 321–333.

——, 1969: The predictability of a flow which possesses many scales of motion. *Tellus,* **21,** 289–307.

Madden, R., and P. Julian, 1994: Observations of the 40-50 day tropical oscillation: A review. *Mon. Wea. Rev.,* **112,** 814–837.

Mann, M. E., and J. Park, 1999: Oscillatory spatiotemporal signal detection in climate studies: A multiple-taper spectral domain approach. *Advances in Geophysics,* Vol. 41, Academic Press, 1–131.

Minetti, J. L., 1991: Study of the climatic singularities in temperature series of Northwest Argentina. Ph.D. thesis., FCEyN-UBA, 117 pp.

——, and W. M. Vargas, 1997: Interaction processes between the annual wave and the disturbances in series of daily temperature. *J. Climate,* **10,** 297–305.

——, and ——, 2005: Regional circulation in Northwest Argentina and related weather conditions. *Weather of Northwest Argentina,* Fundación Caldenius, Editorial Magna, 77–115.

Mo, K., 2001: Adaptive filtering and prediction of intraseasonal oscillations. *Mon. Wea. Rev.,* **129,** 802–817.

Naumann, G., and W. M. Vargas, 2010: Joint diagnostic of the surface air temperature in southern South America and the Madden–Julian oscillation. *Wea. Forecasting,* **25,** 1275–1280.

——, ——, and J. L. Minetti, 2011: Persistence and long-term memories of daily maximum and minimum temperatures in southern South America. *Theor. Appl. Climatol.,* **105,** 341–355.

Penalba, O. C., and W. M. Vargas, 2004: Interdecadal and interannual variations of annual and extreme precipitation over central-northeastern Argentina. *Int. J. Climatol.,* **24,** 1565–1580.

Percival, D. B., and A. T. Walden, 2000: *Wavelet Methods for Time Series Analysis*. Cambridge University Press, 620 pp.

Renwick, J. A., and J. M. Wallace, 1995: Predictable anomaly patterns and the forecast skill of Northern Hemisphere wintertime 500-mb height fields. *Mon. Wea. Rev.,* **123,** 2114–2131.

Schneider, T., and S. M. Griffies, 1999: A conceptual framework for predictability studies. *J. Climate,* **12,** 3133–3155.

Shukla, J., 1981a: Dynamical predictability of monthly means. *J. Atmos. Sci.,* **38,** 2547–2572.

——, 1981b: Predictability of the tropical atmosphere. NASA Tech. Memo. 83829, 51 pp.

——, 1984: Predictability of time averages. Part II: The influence of the boundary forcing. *Problems and Prospects in Long and Medium Range Weather Forecasting,* D. M. Burridge and E. Kallen, Eds., Springer-Verlag, 155–206.

Silvestri, G., and C. Vera, 2009: Nonstationary impacts of the southern annular mode on Southern Hemisphere climate. *J. Climate,* **22,** 6142–6148.

Simmons, A. J., and A. Hollingsworth, 2002: Some aspects of the improvement in skill of numerical weather prediction. *Quart. J. Roy. Meteor. Soc.,* **128,** 647–677.

Sinclair, M. R., J. A. Renwick, and J. W. Kidson, 1997: Low-frequency variability of Southern Hemisphere sea level pressure and weather system activity. *Mon. Wea. Rev.,* **127,** 2531–2542.

Straus, D. M., and J. Shukla, 1981: Global and local fluctuations of winter and summer simulations with the GLAS climate model. NASA Tech. Memo. 83907, 231–236.

Torrence, C., and G. P. Compo, 1998: A practical guide to wavelet analysis. *Bull. Amer. Meteor. Soc.,* **79,** 61–78.

Vargas, W. M., G. Naumann, and J. L. Minetti, 2011: Dry spells in the River Plata basin: An approximation of the diagnosis of droughts using daily data. *Theor. Appl. Climatol.,* **104,** 159–173, doi:10.1007/s00704-010-0335-2.

Vautard, R., P. Yiou, and M. Ghil, 1992: Singular spectrum analysis: A toolkit for short noisy chaotic signals. *Physica D,* **58,** 95–126.

Venzke, S., M. R. Allen, R. T. Sutton, and D. P. Rowell, 1999: The atmospheric response over the North Atlantic to decadal changes in sea surface temperature. *J. Climate,* **12,** 2562–2584.